

FAILURE HANDLING ON A SPLIT-FLAP ULTRALIGHT GENERAL AVIATION AIRCRAFT WITH HYBRID NONLINEAR DYNAMIC INVERSION

Daniel Milz¹, Marc May¹, João Martins^{1,2}, Richard Kuchar¹ & Gertjan Looye¹

¹Deutsches Zentrum für Luft- und Raumfahrt (DLR), Münchner Str. 20, D-82234 Weßling, Germany ²KTH - Royal Institute of Technology, Stockholm, Sweden

Abstract

Ultralight general aviation aircraft provide an accessible gateway to aviation for both manufacturers and pilots. However, due to their reduced weight, requirements, certifications, and costs, these aircraft are more susceptible to hazardous failures than airliners. While they are equipped with a parachute, this is a last resort that is irreversible and can result in a rough landing or the aircraft drifting off. Additionally, the relaxation of medical requirements may result in pilot failures of severe nature. To address these concerns, we propose a semi-electronic flight control concept with split flaps and tailored flight control laws to enable automatic flight during abnormal situations. The simulation results indicate that the closed-loop system performs acceptably in these scenarios. This undermines the intention to use the system in abnormal situations and possibly for augmentation.

Keywords: Flight Control; General Aviation; Ultralight; Dynamic Inversion; Fault-Tolerant Control

1. Introduction

Ultra-light aircraft (ULs) facilitate the entry into aviation by imposing minimal hurdles on both pilots and manufacturers. UL pilots, in particular, are often exempt from extensive training and medical fitness requirements. The certification of a new ULs also entails fewer bureaucratic hurdles and complex certification procedures, which makes it easier for manufacturers. As a result, ULs are becoming increasingly popular in the aviation sports sector. However, this trend comes at the expense of the high safety requirements typical of aviation [1]. This simplification is compensated for by the obligation to have an emergency parachute, which represents the last resort in a critical situation, leading to the destruction of the aircraft. However, this system has additional disadvantages. First, the aircraft is in an uncontrolled descent when the rescue parachute is deployed and can possibly drift into dangerous zones (e.g., high-voltage power lines) under unfavorable wind conditions. Conversely, this system may also fail in the event of a medical emergency or cognitive overload of the pilot. Consequently, there is still a residual risk that needs to be addressed in order to make ultralight aviation safer. The MOREALIS [2] research project addresses this very problem by designing a combined health

monitoring and troubleshooting system for both the pilot and the aircraft. The project pursues the goal of enhancing the safety of ultralight flights by addressing these issues in a larger group with multiple project partners [2]. Scope of *MOREALIS* is the development of an automated emergency landing system, integrated with a comprehensive monitoring system for the pilot and aircraft. The current state of the aircraft condition and the pilot's physiological and cognitive state are fed into an *intervention management* system, that fuses these information and decides whether an emergency landing is triggered. In this case, a vision-based obstacle detection and landing strip selection system is triggered, which forwards the selected landing site to a trajectory planning module, which again forwards the trajectory way-points to an autopilot system. This autopilot system and its flight control laws are the scope of this work.

The flight control system design, including the actuation and sensor selection, are carried out under the strict weight limitation of this ultralight aircraft category (see [2]) and the fact that the system will only be used in emergency situations but not in nominal flight situations. Thus, we decided on a split-flap configuration with simplex electro-mechanical servo motors under the assumption that the pilot can overwrite the control effect anytime through his higher authority. A more detailed description and the analysis of the used split-flap system can be found in [3]. In this split-flap design, the classic control surfaces (i.e., aileron, elevator, and rudder) are each split into two surfaces. One is connected reversibly via cables and rods and used for manual (nominal) control by the pilot. The other part is equipped with simplex electro-mechanical actuators. The control surfaces are split in such a way that the pilot always has more authority than the electric system. This way, an erroneous behavior of the electric system can always be compensated by the pilot. Using this simplex setup requires the flight control laws to be robust to changes in flight dynamics and cope with actuator and sensor failures. Thus, the secondary objective of the flight control laws is the handling of certain failures, which are defined later in more detail.

In [4, 5], the authors present a stability augmentation system based on split control surfaces to obtain two separate automatic and manual flight control systems with the goal of reducing pilot workload and structural loads and improving ride quality [6]. In addition, the overall flight safety is increased. The flight control system must handle the split-flap setup (i.e., cope with simultaneous pilot inputs on the mechanical surfaces) and be robust to failures on the airframe, the sensor, and the actuator system, as well as the propulsion system. This motivates the use of a hybrid nonlinear dynamic inversion-based (hybrid NDI) control law [7, 8, 9] since it compensates for disturbances and can

inversion-based (hybrid NDI) control law [7, 8, 9] since it compensates for disturbances and can handle sensor and actuator failures well. The hybrid NDI law is a combination of the classical NDI with the sensory NDI law, similar to the incremental NDI control law. Although it requires more effort in design, since both sensor information about the aircraft accelerations as well as an on-board model of those dynamics are required, the advantages in minimization of structural loads, handling of (air data) sensor failures, and actuation failures are given [9].

Within the scope of this study, a control law for the ultralight general aviation aircraft *MOREALIS* is conceptualized, designed, and validated. The main focus is on the method of *hybrid NDI* and the allocation of the control surface.

2. Flight Dynamics Model

This the UL research aircraft of *MOREALIS* is described in [2, 3]. Its design and the layout of the split-flap setup is shown in fig. 1, where the ailerons are denoted as δ_a , the elevators as δ_e , the rudder as δ_r , and the flaps as δ_f . The aircraft is equipped with a 33 HP motor driving a propeller. The

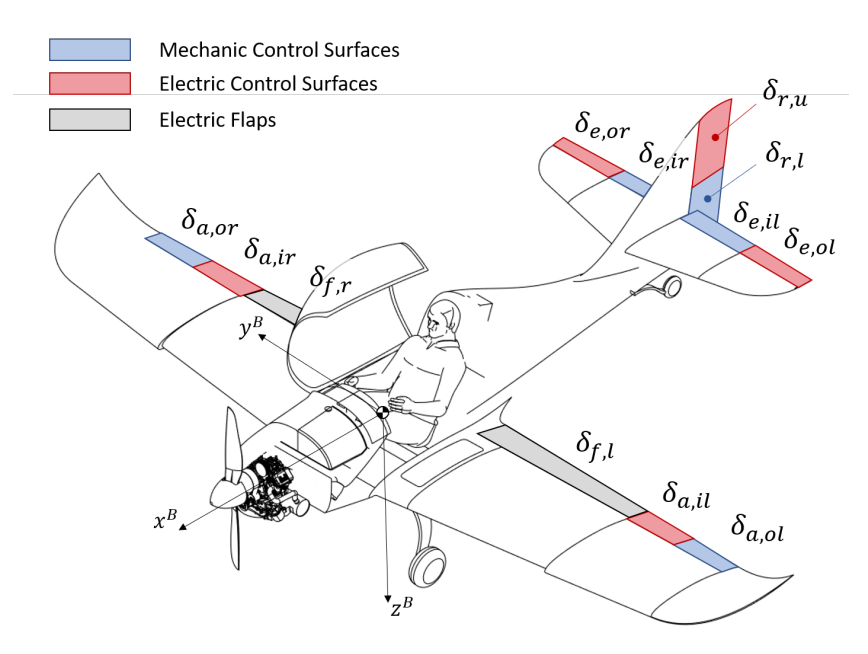


Figure 1 – Concept of mixed flight control layout for the ultralight aircraft.

actuators are simplex electro-mechanical servo motors. The sensor system consists of basic measurements from commercially available instruments. Those cover inertial flight state measurements, basic aerodynamic measurements, and measurements of the electric and mechanical actuators. The flight dynamic model used in the scope of this work is briefly introduced subsequently.

2.1 Flight Dynamic Model

Let the state vector $x \in \mathcal{X} \subset \mathbb{R}^{n_x}$ be represented by r^N denoting the aircraft position in the earth frame, Φ the Euler angle attitude, v^B the aircraft velocity in body frame, and ω^B the angular rates in the body frame. Furthermore, let \mathbb{T}_{NB} and $\mathbb{T}_{\Phi B}$ denote the transformation matrix from body frame to the earth frame or the Euler angle frame, respectively, J the moment of inertia, m the total mass, and f^B and m^B the respective forces and moments in body frame, where the index x denotes the state-dependent quantities, and u the state- and input-dependent ones. Then, the nonlinear state space representation of an aircraft is given as

$$\underbrace{\begin{bmatrix} \dot{r}^{N} \\ \dot{\Phi} \\ \dot{v}^{B} \\ \dot{\omega}^{B} \end{bmatrix}}_{\dot{x}} = \underbrace{\begin{bmatrix} \mathbb{T}_{NB}(\Phi) \ v^{B} \\ \mathbb{T}_{\Phi B}(\Phi) \ \omega^{B} \\ \frac{1}{m} f_{x}^{B}(x) - \omega^{B} \times v^{B} \\ J^{-1} \left(m_{x}^{B}(x) - \omega \times J \omega \right) \end{bmatrix}}_{f(x)} + \underbrace{\begin{bmatrix} 0 \\ 0 \\ \frac{1}{m} f_{u}^{B}(x, T, \delta) \\ J^{-1} m_{u}^{B}(x, T, \delta) \end{bmatrix}}_{g(x, u)} \tag{1}$$

with the smooth mappings $f: \mathbb{R}^{n_x} \mapsto \mathbb{R}^{n_x}$ and $g: \mathbb{R}^{n_x} \times \mathbb{R}^{n_u} \mapsto \mathbb{R}^{n_x}$, and the control actuators δ and the thrust or throttle T forming the input vector $u \in \mathcal{U} \subset \mathbb{R}^{n_u}$. The control surfaces can be separated into two distinct systems: the mechanical (reversible) flight controls

$$\delta_{\mathrm{me}} = \begin{bmatrix} \delta_{\mathrm{a,or}} & \delta_{\mathrm{a,ol}} & \delta_{\mathrm{e,ir}} & \delta_{\mathrm{e,il}} & \delta_{\mathrm{r,l}} \end{bmatrix}$$

and electric flight controls

$$\delta_{el} = \begin{bmatrix} \delta_{a,ir} & \delta_{a,il} & \delta_{f} & \delta_{e,or} & \delta_{e,ol} & \delta_{r,u} \end{bmatrix}$$

with mechanically coupled flaps ($\delta_f = \delta_{f,r} = \delta_{f,l}$). See fig. 1 for a visualization of this setup. The main flight mechanical parameters are stated in table 1. See [3] for a detailed explanation and discussion of the flight dynamic model.

Table 1 – Flight mechanical aircraft data.

Parameter	Parameter Value			
Span width	b	6.40 m		
Mean chord width	c	0.98 m		
Reference surface area	S	$6.71 \mathrm{m}^2$		
Mass	m	250 kg		
		∫ 93 0 −10.4]		
Moment of inertia	J	$\begin{bmatrix} 93 & 0 & -10.4 \\ 0 & 225 & 0 \end{bmatrix} \text{ kg m}^2$		
		$\begin{bmatrix} -10.4 & 0 & 282 \end{bmatrix}$		

Due to the simplex architecture, the failure probability of the aircraft is high. Consequently, it is important consider those in the flight control design. The following failures are defined, implemented in the model, and later investigated:

- · Engine failure leading to an inoperative engine
- Actuator stuck: Electromechanical actuators can fail by staying stuck at their current position
- Loss of effectiveness of the control surfaces can occur due to damage
- Airdata system is prone to failures and can fault completely, leading to an all zeros output

3. Flight Control Law Design

The flight control law design is done for the electrical flight control system, which gets activated in case of emergencies or abnormalities. In case of activation, the system receives flight path commands or waypoint locations from the trajectory generation. The trajectory system calculates a trajectory achievable with the current flight performance and circumvents any obstacles [2]. Thus, the main task of the flight control laws is to use the available electric control surfaces and actuators and track the commanded flight path quantities to the best extent. However, the flight control laws should still be equipped with envelope protections. Given that the system must be capable of tracking a trajectory in abnormal situations, it is acceptable for the system's performance to be reduced in comparison to nominal situations. This especially leads to reduced requirements on flight and control performance parameters, e.g., reduced rise times.

Furthermore, the system has 5 independent control surfaces (i.e., 2 ailerons, 2 elevators and 1 rudder). Thus, a control allocation strategy is required. An optimization-based approach, as shown in [10, 11], is applied but extended with the option the redistribute the control surface commands in case of failures.

Figure 2 shows the control architecture of the implemented control system.

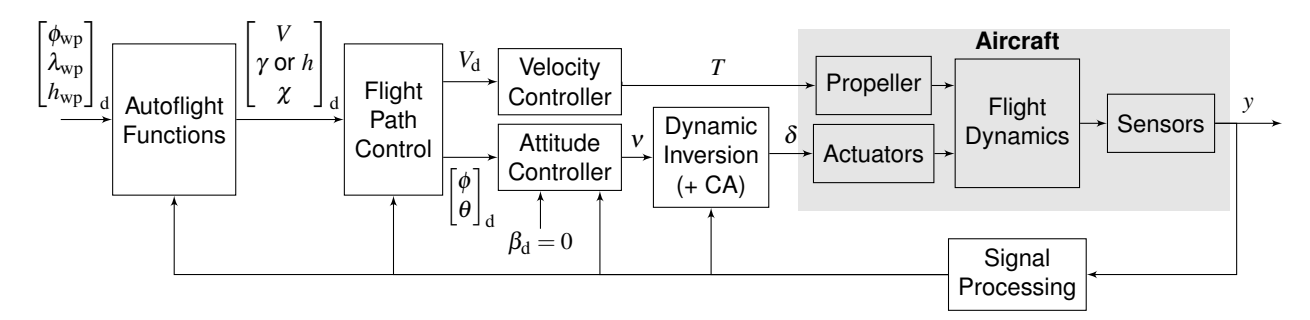


Figure 2 – Control architecture for dynamic inversion-based control system.

3.1 Hybrid Nonlinear Dynamic Inversion

Let $x \in \mathscr{X} \subset \mathbb{R}^{n_x}$ denote the system's state vector, $u \in \mathscr{U} \subset \mathbb{R}^{n_u}$ the input vector, and $y \in \mathbb{R}^{n_y}$ the output vector to be inverted. Furthermore, let $f : \mathbb{R}^{n_x} \mapsto \mathbb{R}^{n_x}$, $g : \mathbb{R}^{n_x} \times \mathbb{R}^{n_u} \mapsto \mathbb{R}^{n_x}$, and $h : \mathbb{R}^{n_x} \mapsto \mathbb{R}^{n_y}$ be smooth vector fields. The index add and (2c) represent additional measurements required for, e.g. state reconstructions. Then, a non-affine nonlinear system can be described by

$$\dot{x} = f(x) + g(x, u) \tag{2a}$$

$$y = h(x) \tag{2b}$$

$$y_{\text{add}} = h_{\text{add}}(x, u) \tag{2c}$$

The hybrid NDI control law for a relative degree of 1 is given by [8, 9]

$$(L_{\hat{v}}h)(\hat{x},u) = v - \mathscr{F}_{compl}(\hat{x},\hat{x},\hat{u})$$
(3)

where $\hat{}$ denotes estimated or measured quantities, $(L_f h)(x)$ the Lie-derivative of h with respect to f, and $v \equiv \hat{y}$. The function $\mathscr{F}_{\text{compl}}$ denotes the result of a complementary filter with the high-pass part being $(L_{\hat{f}}h)(\hat{x})$ representing NDI, and the low-pass part being the sensory NDI approximation $\hat{y} - (L_{\hat{g}}h)(\hat{x},\hat{u})$. The implicit equation (3) can either be solved analytically, by nonlinear equation solvers, or by using local approximations. In the scope of this work, the latter is done. Therefore, the Taylor series approximation is used on the left hand side:

$$(L_{\hat{g}}h)(\hat{x},u) \approx (L_{\hat{g}}h)(\hat{x},\hat{u}) + \frac{\partial (L_{\hat{g}}h)(x,u)}{\partial u}\Big|_{\substack{x=\hat{x}\\ u=\hat{g}}} (u-\hat{u})$$
(4)

This approximation is similar to the incremental NDI law [12, 13] if used with the sensory NDI law alone. A more detailed discussion on this topic is given in [9].

Hybrid NDI combines the properties of sensory NDI and NDI. This leads to a control law that performs well in nominal situations as well as in failure situations for both, (air data) sensor and actuator failures. In this study, an attitude control law is developed (see fig. 2). Thus, the rotational equation of motion

$$\underbrace{\dot{\boldsymbol{\omega}}^{B}}_{\dot{y}} = \underbrace{J^{-1}\left(m_{x}^{B}(x) - \boldsymbol{\omega} \times J\boldsymbol{\omega}\right)}_{\left(L_{f}h\right)(x)} + \underbrace{J^{-1}m_{u}^{B}(x, T, \delta)}_{\left(L_{g}h\right)(x, u)} \tag{5}$$

is used for the inversion. The final control law is then

d for the inversion. The final control law is then
$$\delta = \left(\frac{\partial \hat{m}_{u}^{B}(x,T,\delta)}{\partial \delta}\Big|_{\substack{x=\hat{x} \\ T=\hat{T} \\ \delta=\hat{\delta}}}\right)^{-1} J \cdot \left(\omega_{\text{com}}^{B} - \mathscr{F}_{\text{compl}} - J^{-1}\hat{m}_{u}^{B}(\hat{x},\hat{T},\hat{\delta}) + J^{-1} \frac{\partial \hat{m}_{u}^{B}(x,T,\delta)}{\partial \delta}\Big|_{\substack{x=\hat{x} \\ T=\hat{T} \\ \delta=\hat{\delta}}} \hat{\delta}\right) \tag{6}$$

with the complementary filtered (κ) function

$$\mathscr{F}_{\text{compl}} = \kappa \left\{ \begin{array}{ll} J^{-1} \left(\hat{m}_{x}^{B}(\hat{x}) - \hat{\omega} \times J \hat{\omega} \right), & \text{high-pass} \\ \hat{\omega}^{B} - J^{-1} \hat{m}_{u}^{B}(\hat{x}, \hat{T}, \hat{\delta}), & \text{low-pass} \end{array} \right.$$
(7)

In this study, we use a first-order complementary filter with a cutoff frequency of 5 rad s⁻¹.

3.2 Control Allocation Strategy

The control allocation problem becomes relevant when the number of inputs is greater than the number of outputs intended for control $(n_u > n_v)$. Moreover, assuming that actuator failures can be detected, control allocation methods are able to further improve failure handling of an aircraft by allowing a reconfiguration and redistribution of the current deflections. The strategy will be an optimization-based approach as in [11, 10]. Assuming an objective function quadratic in u, $L(\hat{x}, \delta, u)$, to be minimized. Then, the problem is formulated as

$$\min_{\substack{u \in \mathscr{U} \\ \text{s.t.}}} L(\hat{x}, \hat{\delta}, u) := L_0(\hat{x}, \hat{\delta}) + L_1(\hat{x}, \hat{\delta})u + u^T L_2(\hat{x}, \hat{\delta})u \\
\text{s.t.} \qquad \hat{M}_u u = v - \hat{f}_{\text{compl}} - J^{-1} \hat{m}_u^B(\hat{x}, \hat{T}, \hat{\delta}) + \hat{M}_u \hat{\delta} := \tau$$
(8)

where $L_0(\hat{x}, \hat{u}) \in \mathbb{R}$ is a scalar, $L_1(\hat{x}, \hat{u}) \in \mathbb{R}^{n_u}$ is a row vector, $L_2(\hat{x}, \hat{u}) = L_2(\hat{x}, \hat{u})^T \succ 0 \in \mathbb{R}^{n_u \times n_u}$ is a symmetric positive definite matrix, \hat{M}_u as defined in (6), and $v \equiv \dot{\omega}_{\text{com}}^B$ is the virtual control input. Note that the quadratic objective function assumption does not impose any strict limitation on this function as it can always be approximated by a second-order Taylor series expansion to reach the form in (8). The solution to (8) has the following form

$$u = \hat{M}_{u}^{+} \tau + \frac{1}{2} \left(\hat{M}_{u}^{+} \hat{M}_{u} - I \right) L_{2}(\hat{x}, \hat{\delta})^{-1} L_{1}(\hat{x}, \hat{\delta})^{T}$$
(9)

where $\hat{M}_u^+ = L_2(\hat{x},\hat{\delta})^{-1}\hat{M}_u^T \left(\hat{M}_u L_2(\hat{x},\hat{u})^{-1}\hat{M}_u^T\right)^{-1}$ is the weighed pseudo-inverse of \hat{M}_u . As stated in [8, 10], the first term in eq. (9) relates to the primary goal, which is the inversion of the plant dynamics. The second term relates to the goal of minimizing the objective function $L(\hat{x}, \hat{\delta}, u)$. In fact, as the second term is in the null space of \hat{M}_u , it will not influence in anyway the primary goal.

In order to improve failure handling, it is first assumed that actuator failures can be detected instantaneously. Modifications to the theory will be made to better handle these failures when they happen. The common failure case that will be considered is when actuators get stuck at a certain deflection. Let S be the set of indexes of the stuck actuators, $S = \{s_1, \dots, s_{n_S}\}$ where $0 \le n_S \le n_u$ is the number of stuck actuators and each $s_i \in \{0, 1, \dots, n_u\}$ represents the index of a stuck actuator. Similarly, $W = \{s_1, \dots, s_{n_u}\} \setminus S$ corresponds to the complementary set of the indexes S, which corresponds to the working actuators. With these definitions, u_S becomes the vector of stuck elements. In the same way, u_W becomes the vector of working actuators. Moreover, $\hat{M}_{u_{S|}}$ becomes the control effectiveness matrix with only the columns corresponding to the stuck actuator indexes, and $\hat{M}_{u_{W_1}}$ vice versa. Note that the constraint equation in (8) must still hold to correctly invert the plant. The constraint equation can be rewritten by separating \hat{M}_u and u with the new quantities defined

$$\hat{M}_{u_{W|}} u_{W} = v - \hat{f}_{\text{compl}} - J^{-1} \hat{m}_{u}^{B}(\hat{x}, \hat{T}, \hat{\delta}) + \hat{M}_{u} \hat{\delta} - \hat{M}_{u_{S|}} u_{S}
= v - \hat{f}_{\text{compl}} - J^{-1} \hat{m}_{u}^{B}(\hat{x}, \hat{T}, \hat{\delta}) + \hat{M}_{u_{W|}} \hat{\delta}_{W}$$
(10)

where, for simplification, it was noted that $u_S = \hat{\delta}_S$.

The optimization problem presented in (8) corresponds to an aircraft flying free of failures. However, when certain actuators get stuck, u_S becomes fixed and the subset for the minimization variable u is no longer \mathscr{U} . Thus, the formulation of problem (8) needs to be slightly altered by replacing u_W as the minimization variable.

By making use of the row vectors $L_{1_S}(\hat{x},\hat{\delta})$ and $L_{1_W}(\hat{x},\hat{\delta})$, which represent the parts of L_1 corresponding to the stuck and working actuators, respectively. Additionally, letting $L_{2_{SW}}(\hat{x},\hat{\delta})$, $L_{2_{WS}}(\hat{x},\hat{\delta})$, $L_{2_{WW}}(\hat{x},\hat{\delta})$ and $L_{2_{SS}}(\hat{x},\hat{\delta})$ represent the parts of L_2 corresponding to the subset of working or stuck actuators., and noting that $L_{2_{SW}}(\hat{x},\hat{\delta}) = L_{2_{WS}}^T(\hat{x},\hat{\delta})$, the objective function can be written as

$$L(\hat{x}, \hat{\delta}, \hat{\delta}_{S}, u_{W}) = \bar{L}_{0}(\hat{x}, \hat{\delta}, \hat{\delta}_{S}) + \bar{L}_{1}(\hat{x}, \hat{\delta}, \hat{\delta}_{S})u_{W} + u_{W}^{T}\bar{L}_{2}(\hat{x}, \hat{\delta}, \hat{\delta}_{S})u_{W}$$

$$\tag{11}$$

where

$$\bar{L}_0(\hat{x}, \hat{\delta}, \hat{\delta}_S) = L_0(\hat{x}, \hat{\delta}) + L_{1s}(\hat{x}, \hat{\delta})\hat{\delta}_S + \hat{\delta}_S^T L_{2ss}(\hat{x}, \hat{\delta})\hat{\delta}_S$$
(12a)

$$\bar{L}_1(\hat{x}, \hat{\delta}, \hat{\delta}_S) = L_{1_W}(\hat{x}, \hat{\delta}) + 2\hat{\delta}_S^T L_{2_{SW}}(\hat{x}, \hat{\delta})$$
(12b)

$$ar{L}_2(\hat{x},\hat{\delta},\hat{\delta}_S) = L_{2_{WW}}(\hat{x},\hat{\delta})$$
 (12c)

Let $\mathscr{U}_W \subseteq \mathscr{U}$ denote the working subset of \mathscr{U} . Then, the optimization problem that includes actuator failure compensation is given as

$$\min_{\substack{u_W \in \mathscr{U}_W \\ \text{s.t.}}} L(\hat{x}, \hat{\delta}, \hat{\delta}_S, u_W) = \bar{L}_0(\hat{x}, \hat{\delta}, \hat{\delta}_S) + \bar{L}_1(\hat{x}, \hat{\delta}, \hat{\delta}_S) u_W + u_W^T \bar{L}_2(\hat{x}, \hat{\delta}, \hat{\delta}_S) u_W \\
\text{s.t.} \qquad \hat{M}_{u_W} u_W = v - \hat{f}_{\text{compl}} - J^{-1} \hat{m}_u^B(\hat{x}, \hat{T}, \hat{\delta}) + \hat{M}_{u_W} \hat{\delta}_W := \bar{\tau}$$
(13)

This problem can be solved similar to the original one in (8), leading to an allocation of u_W , i.e.,

$$u_W = \hat{\bar{M}}_{u_{W|}}^+ \bar{\tau} + \frac{1}{2} \left(\hat{\bar{M}}_{u_{W|}}^+ \hat{M}_{u_{W|}}(\hat{x}) - I \right) \bar{L}_2(\hat{x}, \hat{\delta}, \hat{\delta}_S)^{-1} \bar{L}_1(\hat{x}, \hat{\delta}, \hat{\delta}_S)^T$$
(14)

where $\hat{\bar{M}}_{u_{W|}}^{+} = \bar{L}_{2}(\hat{x}, \hat{\delta}, \hat{\delta}_{S})^{-1} \hat{M}_{u_{W|}}^{T} \left(\hat{M}_{u_{W|}} \bar{L}_{2}(\hat{x}, \hat{\delta}, \hat{\delta}_{S})^{-1} \hat{M}_{u_{W|}}^{T} \right)^{-1}$.

3.3 Attitude Controller

The attitude controller is implemented as shown in [14, 15, 16].

The attitude controller tracks the Euler angle attitude Φ via the body angular accelerations $\dot{\omega}$, which are inverted in the hybrid NDI core. The angular accelerations are tracked through the dynamic inversion with the virtual control inputs v_{ϕ} and v_{θ} , which are the Euler accelerations and transformed into v_p and v_q via kinematic relations, and v_r . The control law is given as

$$\begin{bmatrix} v_{\phi} \\ v_{\theta} \end{bmatrix} = \left(\left(K_{p} + \frac{K_{i}}{s} \right) \left(\begin{bmatrix} \phi_{d} \\ \theta_{d} \end{bmatrix} - \begin{bmatrix} \hat{\phi} \\ \hat{\theta} \end{bmatrix} \right) + K_{d} \left(\begin{bmatrix} \dot{\phi}_{d} \\ \dot{\theta}_{d} \end{bmatrix} - \begin{bmatrix} \hat{\phi} \\ \hat{\theta} \end{bmatrix} \right) + K_{ff} \begin{bmatrix} \ddot{\phi}_{d} \\ \ddot{\theta}_{d} \end{bmatrix} \right)$$
(15)

$$v_r = \left(K_p + \frac{K_i}{s}\right)(r_d - \hat{r}) \tag{16}$$

with the notation $\begin{bmatrix} p & q & r \end{bmatrix}^T = \omega$ and controller gains K. The desired roll and pitch angles and derivatives are calculated through a second-order reference model as shown in Figure 3 with the damping ζ and frequency ω_0 . The reference model includes the option for Pseudo Control Hedging (PCH) [17] through the input $\begin{bmatrix} \ddot{\phi} & \ddot{\theta} \end{bmatrix}_{hdg}^T$.

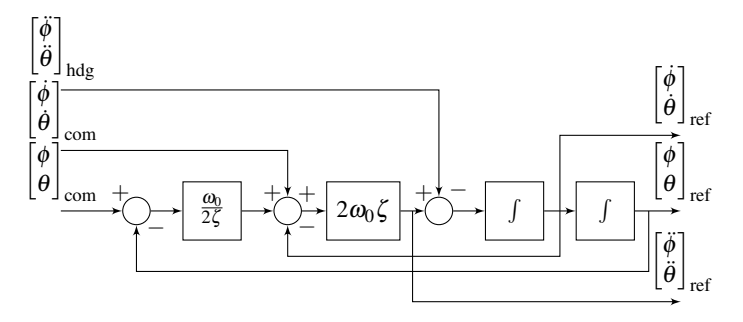


Figure 3 – Second-order reference model architecture

The sideslip controller implements the following law

$$r_{\rm c} = \hat{\beta} - \left(\frac{K_{\rm i,\beta}}{s} \left(\beta_{\rm d} - \hat{\beta}\right) - K_{\rm p,\beta} \hat{\beta}\right) \tag{17}$$

with the estimated sideslip angle derivative $\hat{\hat{\beta}}$ using $v_z \approx V_{tas} \alpha$:

$$\hat{\beta} = \frac{\hat{v}_z \, \hat{p} - F_y}{\hat{V}_{tas}} \approx \hat{\alpha} \, \hat{p} - \frac{F_y}{\hat{V}_{tas}} \approx \hat{\alpha} \, \hat{p} - \frac{g \, \hat{a}_y}{\hat{V}_{tas}} \tag{18}$$

The turn coordination $v_{r,tc}$ that corrects v_r with the rotation generated by a roll maneuver is given as

$$v_{r,tc} pprox \ddot{\psi}_c = 2\left(\frac{g \tan \phi_c}{\hat{V}} - \hat{\psi}\right)$$
 (19)

3.4 Flight Path Controller

Aim of the flight path controller is the tracking of altitude h or the flight path angle γ through the pitch angle θ , the course χ via the roll angle ϕ , while keeping $\beta=0$, and the airspeed $V_{\rm tas}$ via the autothrottle.

The commanded roll angle ϕ_c needed to track the desired course χ_d can be calculated as

$$\phi_{\rm c} = K_{\chi} \frac{\hat{V}}{g} \left(\chi_{\rm d} - \hat{\chi} \right) \tag{20}$$

with $K_{\chi} \approx 0.05$.

The commanded flight path angle γ_c that allows tracking the desired altitude h_d can be calculated as

$$\gamma_{\rm c} = \frac{1}{\hat{V}} K_{\rm h} \left(h_{\rm d} - \hat{h} \right) \tag{21}$$

with $K_{\rm h} \approx 0.1$.

This flight path angle can be tracked by an pitch angle command θ_c , given as

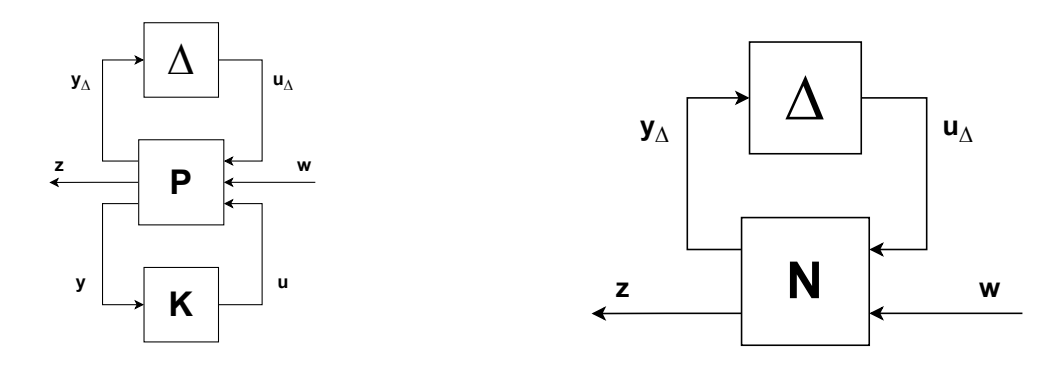
$$\theta_{c} = \frac{K_{\gamma}}{s} (\gamma_{c} - \hat{\gamma}) - \frac{1}{\tau_{\theta}} \hat{\gamma}$$
 (22)

with $K_{\gamma} \approx 0.4$ and $\frac{1}{\tau_{\theta}} \approx 0.7$.

3.4.1 Autothrottle

The autothrottle tracks a velocity command by adjusting the engine throttle. It is mainly feedback controller on airspeed, but can optionally use an additional feedforward input from flight path angle commands. Figure 4 shows the block diagram of the used auto-throttle function. The gains are chosen as $K_V \approx 0.15$, $K_{\dot{V}} \approx 0.3$, and $K_{\ddot{V}} \approx 0.7$.

Figure 4 – Block diagram of the autothrottle control law.



- (a) System structure for controller analysis.
- (b) $N\Delta$ -structure for robust performance analysis.

Figure 5 – System structures for robust control design.

3.5 Robust Control

As the controller has to cope with limited authority, model uncertainties, disturbances, or failures, robust control design and analysis is employed. Figure 5a shows the classical ΔPK structure of a robust system with uncertainties Δ , where $||\Delta||_{\infty} \leq 1$, the controller K and the plant P.

The measurements y and control inputs u are pulled to have the controller K as a separate block. Moreover, the disturbances w and performance signals z are chosen and scaled appropriately so that robustness can be checked. It is convenient for the closed-loop system analysis to combine P and K to form the $N\Delta$ -structure, as it can be seen in fig. 5b, with

$$\begin{bmatrix} y_{\Delta} \\ z \end{bmatrix} = \underbrace{\begin{bmatrix} N_{11} & N_{12} \\ N_{21} & N_{22} \end{bmatrix}}_{N} \begin{bmatrix} u_{\Delta} \\ w \end{bmatrix}$$
 (23)

where y_{Λ} is the input to the uncertainty scaling and u_{Λ} the output.

Before presenting the requirements for stability and performance, the Structured Singular Value, μ , needs to be defined:

$$\mu_{\Delta}(N)^{-1} := \min\{\bar{\sigma}(\Delta) : \det(I - N\Delta) = 0 \text{ for structured } \Delta\}$$
 (24)

This can be thought as the reciprocal of how big that structured uncertainty Δ can be before the matrix $I-N\Delta$ becomes singular. Note that $\mu_{\Delta}(N)$ is a function of the system M, the structured uncertainty Δ , and the frequency ω .

As explained more thoroughly in [18], the requirements for stability and performance are:

- Nominal Stability: N is internally stable
- Nominal Performance: $||N_{22}||_{\infty} < 1$ and nominal stability
- Robust Stability: $\mu_{\Delta}(N_{11}) < 1, \forall \omega$ and nominal stability
- Robust Performance: $\mu_{\tilde{\Delta}}(N) < 1, \forall \omega, \tilde{\Delta} = \begin{bmatrix} \Delta & 0 \\ 0 & \Delta_P \end{bmatrix}$ and nominal stability

where Δ_P is a $n_w \times n_z$ complex uncertainty.

The computation of the structured singular values can be inefficient, since it is necessary to search through all possible Δ . Therefore, a tight upper bound for μ is used to detect the requirements [18, 19]

$$\mu_{\tilde{\Delta}}(N) \le \min_{D \in \mathscr{D}_{\tilde{\lambda}}} \bar{\sigma}(DND^{-1}) \tag{25}$$

where $\mathcal{D}_{\tilde{\Lambda}} := \{D : D\Delta = \Delta D\}.$

3.5.1 Robustness Design

This robust design was done for the linearized model of the system with the same controller structure as presented in Section 3.3. The linearized model *P* can be seen in fig. 6

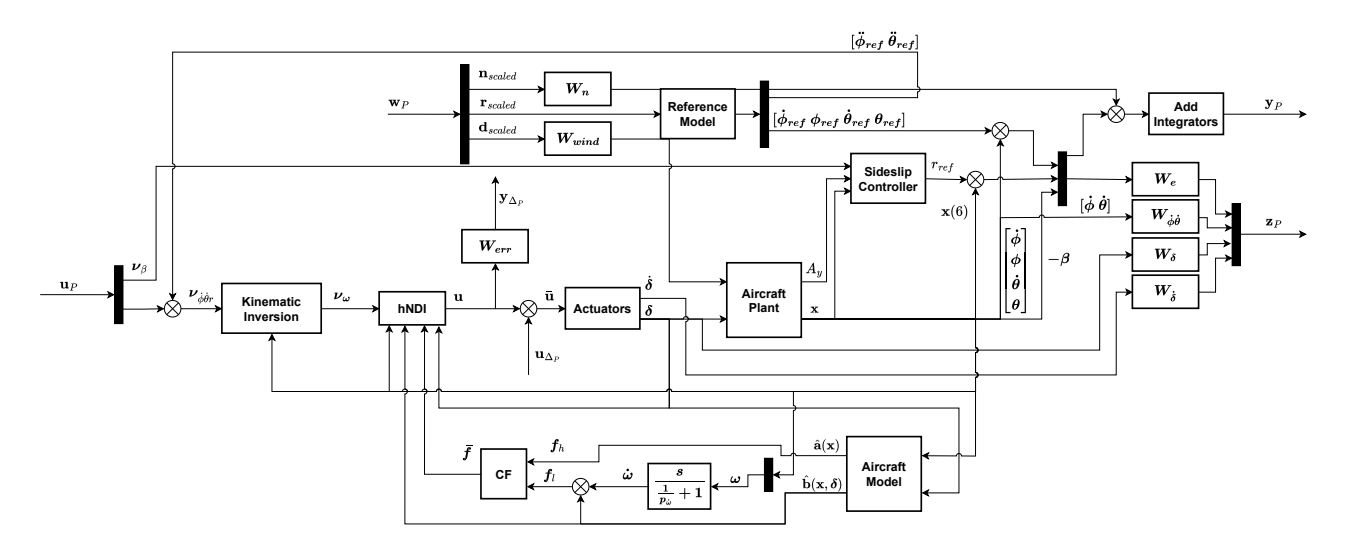


Figure 6 – Interconnection structure of liner system P used for μ -synthesis.

The inputs are denoted as u_{Δ_P} , w_P and u_P , and the outputs as y_{Δ_P} , z_P and y_P . The signals u_{Δ_P} and y_{Δ_P} correspond to the output and input of the unitary uncertainty block Δ . Taking into account where these signals enter and leave the system P, the uncertainty is an additive uncertainty on the input side of the actuator. Moreover, the uncertainty block Δ is a diagonal block with unitary complex uncertainties χ_i for i=1,...,5.

$$\Delta = \begin{bmatrix} \chi_1 & 0 & 0 & 0 & 0 \\ 0 & \chi_2 & 0 & 0 & 0 \\ 0 & 0 & \chi_3 & 0 & 0 \\ 0 & 0 & 0 & \chi_4 & 0 \\ 0 & 0 & 0 & 0 & \chi_5 \end{bmatrix}; \quad \chi_i \in \mathbb{C} : |\chi_i| < 1, \text{ for } i = 1, ..., 5$$
 (26)

With this uncertainty modeling, the uncertainty would be propagated through the system and it can be argued that no other uncertainty is required. Moreover, adding more uncertainties had the disadvantage of making the overall linear system more complex leading to a harder μ -synthesis problem to solve. Regarding the input u_P and the output y_P , these connect to the controller K.

For the disturbances w_P and the performance signals z_P , only relevant quantities were considered in order to have suitable results while not making the problem too complex. Starting with the first disturbance, it can be seen from the diagram in fig. 6, that noise was modeled to enter the output that goes to the controller. The corresponding weight W_n goes to 0 for small frequencies and is big for higher frequencies than the bandwidth of the reference model, similar to a high-pass filter. The magnitude plots of this and the rest of the weights that are not constant are presented in fig. 7. This weight had the importance of making K ineffective at high frequencies. The reference commands were also considered as a disturbance, in this way, the aircraft achieves performance for multiple reference signals. The last disturbance considered is wind gusts. Wind gusts are typically very slow disturbances as stated in [20], therefore, a low pass filter was chosen with a low crossover frequency.

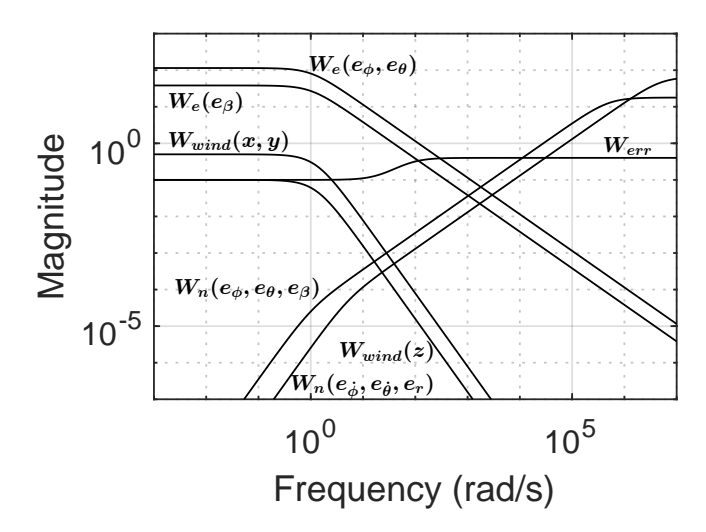


Figure 7 – Magnitude plot of the weights used for μ -synthesis.

Having shown the disturbances considered, the performance signals z_P describe the intended behavior for the aircraft. The first grabs the three angle errors of roll, pitch and sideslip, and weights them with a low-pass filter W_e . This was done to relieve this objective past the system's reference bandwidth. For the roll and pitch angular rates, the constant weight

$$W_{\dot{\phi}\,\dot{ heta}} = \left[rac{5\pi}{180}^{-1} rac{5\pi}{180}^{-1}
ight]$$

was chosen. For the controller deflections δ and rates $\dot{\delta}$, constant weights

$$W_{\delta} = \frac{3}{2} \left[\delta_{a,ir_{\mathsf{max}}}^{-1} \ \delta_{a,il_{\mathsf{max}}}^{-1} \ \delta_{e,or_{\mathsf{max}}}^{-1} \ \delta_{e,ol_{\mathsf{max}}}^{-1} \ \delta_{r,up_{\mathsf{max}}}^{-1} \right]$$

and

$$W_{\dot{\delta}} = \frac{1}{2} \left[\dot{\delta}_{a,ir_{\mathsf{max}}}^{-1} \ \dot{\delta}_{a,il_{\mathsf{max}}}^{-1} \ \dot{\delta}_{e,or_{\mathsf{max}}}^{-1} \ \dot{\delta}_{e,ol_{\mathsf{max}}}^{-1} \ \dot{\delta}_{r,up_{\mathsf{max}}}^{-1} \right]$$

were used. Regarding the weight W_{err} involved with the uncertainties, this one was set to around 0.1 for low frequencies while being around 0.4 for high frequencies.

4. Results

Subsequently, the performance of the proposed controller and flight control concept is evaluated by means of performance, failure handling, robustness to uncertainties, and disturbance rejection. The analyses are carried out on the nonlinear 6-DoF model [3].

4.1 Robust Performance and Stability

From the linear analysis results of the system, the controller achieves nominal stability by design. Furthermore, nominal performance is achieved as $||N_{22}||_{\infty}=0.666<1$. Figure 8a shows the corresponding singular values: The highest singular value is still below 1 for all frequencies. Figure 8b shows the frequency plot for $\mu_{\Delta}(N_{11})$ indicating robust stability as it is always below 1, and in fact $\max\left(\mu_{\Delta}(N_{11})\right) \leq 0.630$. Finally, robust performance is also achieved, $\max\left(\mu_{\tilde{\Delta}}(N)\right) \leq 0.922$. The corresponding frequency plot is depicted in fig. 8c: Robust performance is achieved since $\mu_{\tilde{\Delta}}(N)(j\omega) < 1$ for all ω . The iteratively determined values for the uncertainties are: For low frequencies, 10% of uncertainty for all actuator inputs and they rose to 40% for high frequencies.

Additionally, for comparison reasons, an unstructured controller K_{uns} was considered. To do this, the output was modified to only include the error for roll, pitch and the angular rate r, and the input to only have the corresponding virtual inputs. The sideslip error and its corresponding virtual control was removed because there are some redundancies between them. This comes from the fact that r_{ref} , which belonged to the output of the controller is a function of v_{β} , which was part of the inputs. Moreover, the sideslip controller structure is something that is used commonly. After doing again

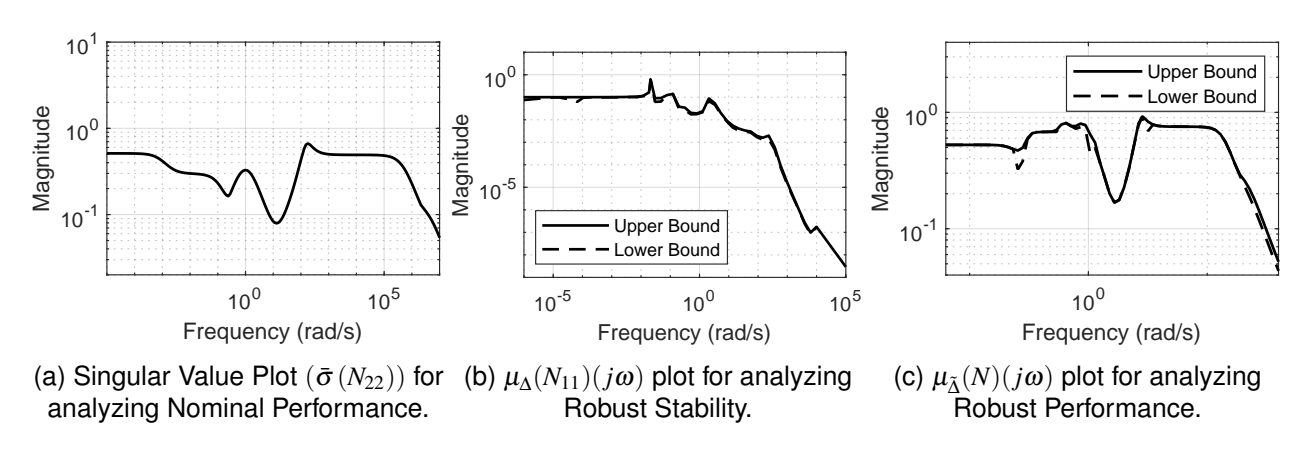


Figure 8 – Nominal and robust performance and robust stability plots.

the $\mu-$ synthesis, this time the system was able to achieve lower values for the structured singular value. After using Hankel model reduction to remove weakly controllable/observable states, the total number of states went from 90 to 30 and the new value for the structured singular value was found to be $\max{(\mu_{\tilde{\Delta}}(N))} \leq 0.717$, which is around 0.2 less than the structured approach Furthermore, to check if the unstructured controller had cross coupling terms, input to output peak gains were checked. This can be seen in table 2.

Table 2 – Input to output peak gains of unstructured robust controller

	e_{ϕ}	e_{θ}	e_r
ν_{ϕ}	96.4	0.79	11.7
v_{θ}	13.6	77	0.2
v_r	3.04	0.5	17.6

4.2 Nominal Performance, Transients and Control Allocation

As the system will likely engage during maneuvers or non-trimmed conditions, a flight state with non-zero mechanical surface deflections is present at the start. For the first experiment, a turn maneuver is assumed, whereas for the second experiment a climb maneuver is flown by the pilot. After $5\,\mathrm{s}$, the autopilot system is triggered, which upon enabling should keep the current flight state in order to avoid hard maneuvers.

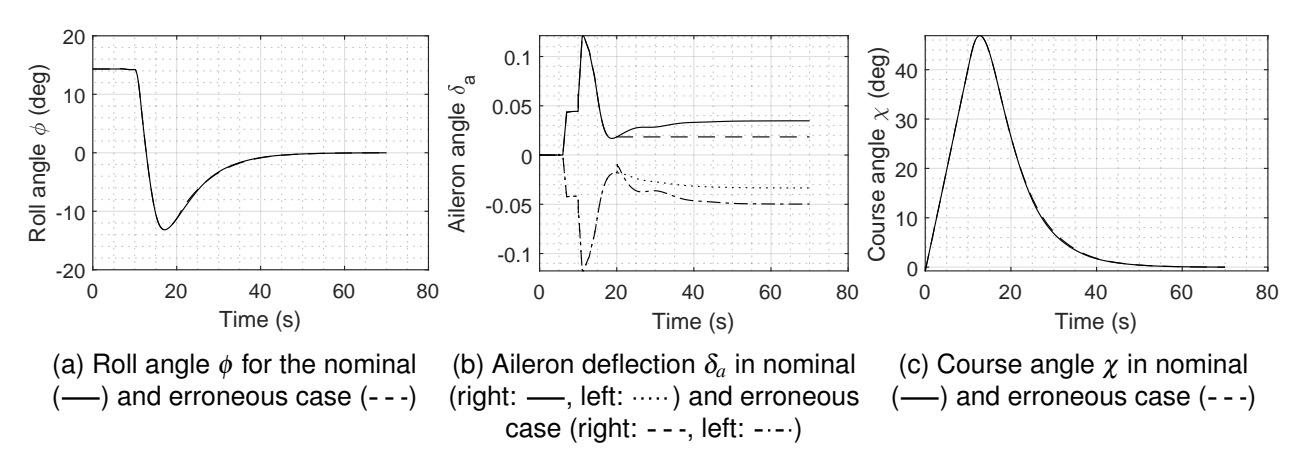


Figure 9 – Lateral experiment for nominal performance, transients, and control reallocation.

Simultaneously, the trajectory planning is triggered but is expected to take $5\,\mathrm{s}$ in this experiment until an optimal trajectory is found. During this time (at $6\,\mathrm{s}$), the pilot releases the stick and the mechanic control surfaces converges to zero deflection (until $7\,\mathrm{s}$). After a trajectory is found (at $10\,\mathrm{s}$), the controller is expected to performs a change in course ($\chi=0^\circ$) or a change in flight level

 $(h=400\,\mathrm{m})$. During the maneuver (at $20\,\mathrm{s}$) the right aileron or the right elevator fails and gets stuck. This is detected by a FDIR algorithm and instantaneously compensated in the control allocation, which performs a reconfiguration of the control surfaces to cope with the failure. The results of the lateral experiment are depicted in fig. 9 and the results of the longitudinal experiment are shown in fig. 10.

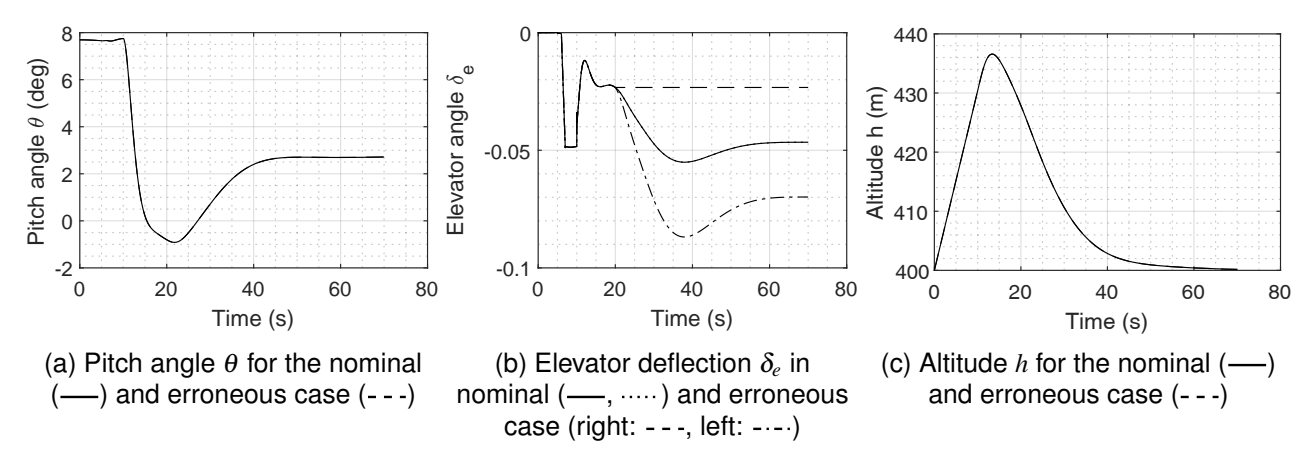


Figure 10 – Longitudinal experiment for nominal performance, transients, and control reallocation.

4.3 Robustness to Model Uncertainties

In order to evaluate the robustness to model uncertainties, the following experiment is conducted: First steps in the roll angle (30° at $10 \, \mathrm{s}$ and 0° at $30 \, \mathrm{s}$) are tracked and afterward steps in pitch angle (from the trimmed state to 10° at $50 \, \mathrm{s}$ and 0° at $70 \, \mathrm{s}$) are tracked. This experiment is done in a montecarlo simulation and repeated several times with randomly sampled model uncertainties according to table 3. In the table, $\mathcal{N}(\mu, \sigma)$ denotes a normal probability distribution with mean μ and standard deviation σ . The results are depicted in fig. 11. The figures show the nominal response with the standard error of the monte-carlo results compared to the nominal response.

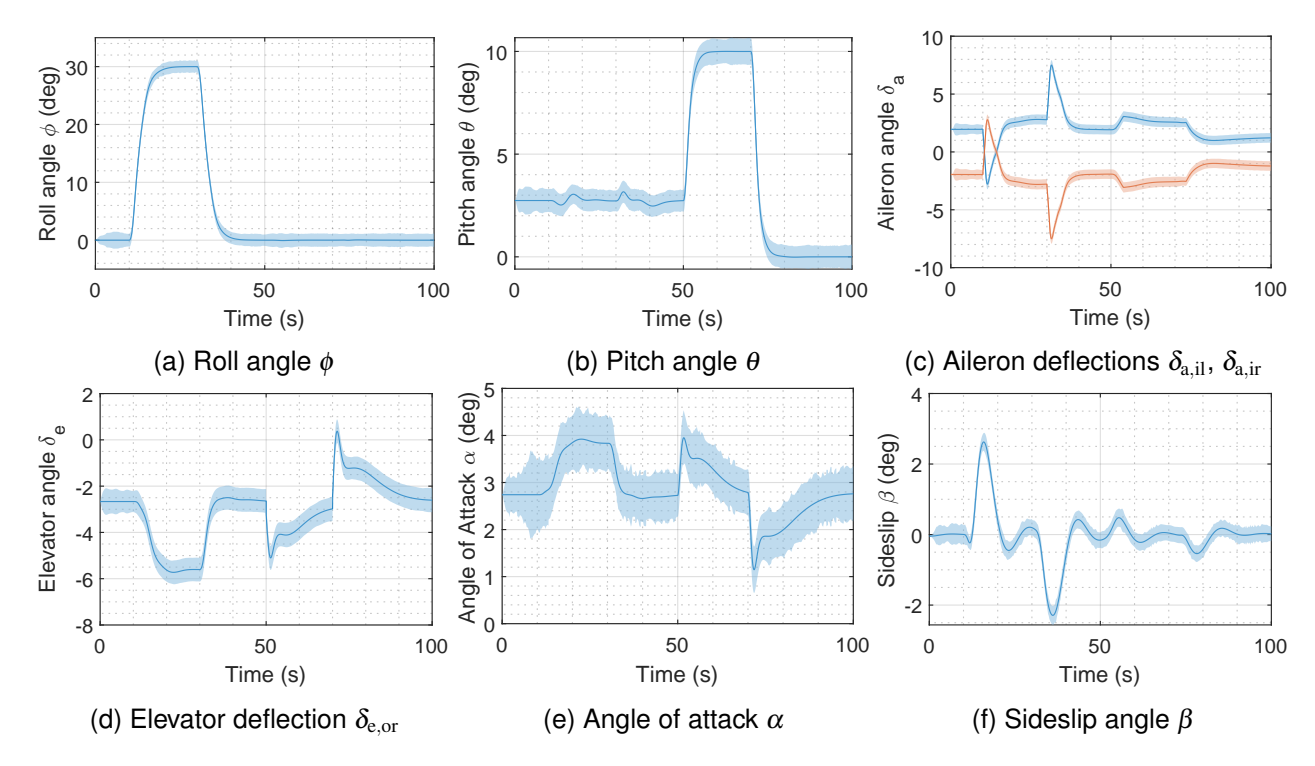


Figure 11 – Monte-carlo simulation of lateral and longitudinal maneuvers with sampled uncertainties.

Table 3 – Uncertainties used in the monte-carlo simulation.

Name	Symbol	Probability Distribution
Multiplicative	ΔC_D	$\mathcal{N}(1,0.1)$
aerodynamic force	ΔC_Y	$\mathcal{N}(1,0.1)$
uncertainty	ΔC_L	$\mathcal{N}(1,0.1)$
Additive	ΔC_D	$\mathcal{N}(0,0.05)$
aerodynamic force	ΔC_Y	$\mathscr{N}(0,0)$
uncertainty	ΔC_L	$\mathcal{N}(0,0.05)$
Multiplicative	ΔC_l	$\mathcal{N}(1,0.1)$
aerodynamic	ΔC_m	$\mathcal{N}(1,0.1)$
moment uncertainty	ΔC_n	$\mathcal{N}(1,0.1)$

Name	Symbol	Probability Distribution
Additive center of gravity uncertainty	$\Delta x_{\rm cg}$ $\Delta y_{\rm cg}$	$ \begin{array}{ c c } \mathcal{N}(0,0.1) \\ \mathcal{N}(0,0.05) \end{array} $
	$\Delta z_{\rm cg}$	$\mathcal{N}(0,0.05)$
Add. mass unc.	Δm	$\mathcal{N}(0,0.1)$
Multiplicative inertia uncertainty	$\Delta I_{\rm xx}$	$\mathcal{N}(1,0.1)$
	$\Delta I_{ m yy}$	$\mathcal{N}(1,0.1)$
	ΔI_{zz}	$\mathcal{N}(1,0.1)$
	$\Delta I_{\rm xz}$	$\mathcal{N}(1,0.1)$
	ΔI	$\mathcal{N}(1,0.1)$

4.4 Disturbances from Turbulence

This experiment evaluates the disturbance rejection characteristics of the proposed control system. Therefore, disturbances in the form of wind velocities $d_{\rm V_w^B}$ are considered. The wind field is represented by a Dryden continuous turbulence according to MIL-STD-1797A with a frequency of $10\,{\rm Hz}$ and a probability of exceedance of 10^{-2} and increasing (every $20\,{\rm s}$) wind speeds from $0\,{\rm m\,s^{-1}}$ to $10\,{\rm m\,s^{-1}}$. The results are shown in fig. 12. The figures show the nominal response with the standard error of the monte-carlo results compared to the nominal response.

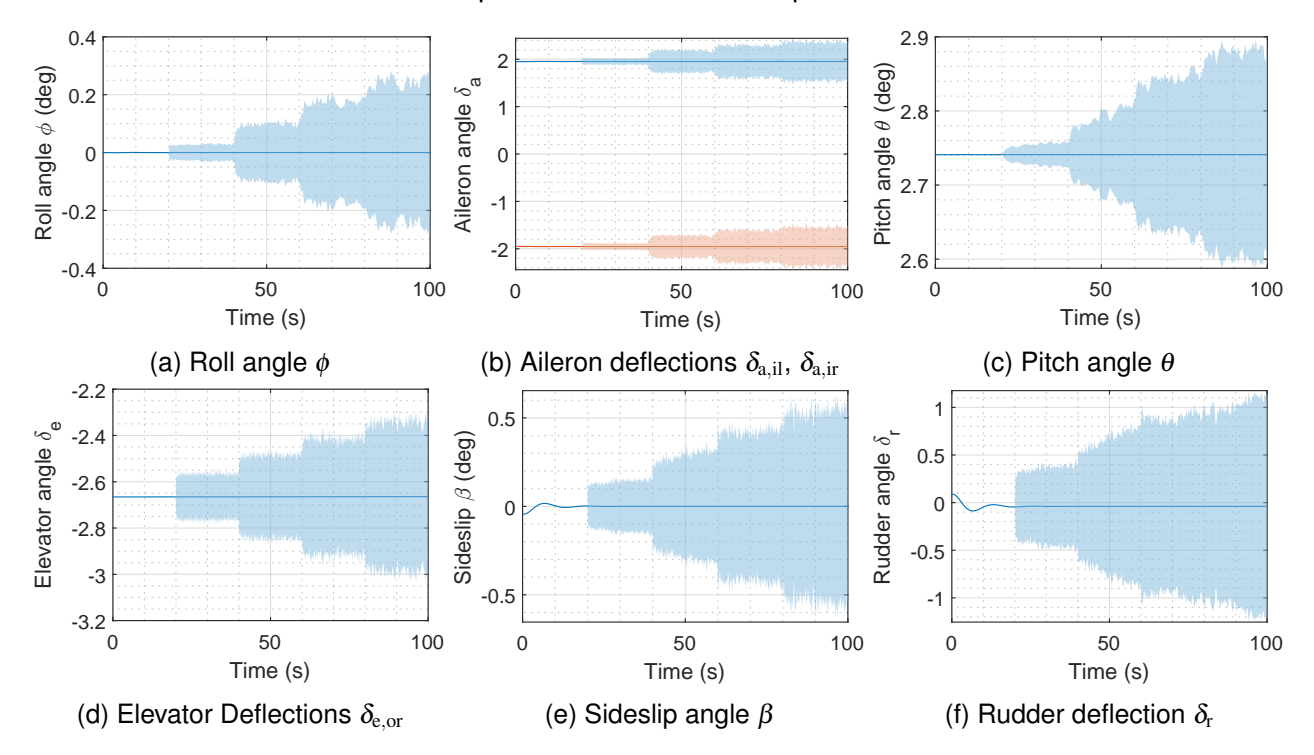


Figure 12 – Monte-carlo simulation of steady flight under increasing Dryden continuous turbulences.

5. Discussion

The goal of this work is developing a flight control system for automated flight of an ultralight aircraft in case of medical or aircraft emergencies. Thus, the requirements do not focus on achieving a flight control system with the performance and robustness of a full fly-by-wire system, but to achieve enough performance to fly maneuvers necessary to automatically land the aircraft. Therefore, we applied a hybrid NDI control law with optimization-based control allocation and reconfiguration in case of control surface failures. Furthermore, robust control design is used to tune controller gains appropriately. The finally proposed control law is analyzed by means of robust performance and stability analysis as well as time-domain simulations.

Section 4.1 shows the result of the robust performance and stability analysis. The results indicate that nominal performance and stability are achieved and that the system can handle disturbances and uncertainties in the model while still maintaining performance. Robust stability and performance is achieved within the determined ranges of uncertainties. Those are, however, narrow in the low-frequency domain. This is an issue for a nominal configuration, and also this configuration. The comparably low uncertainties that can be handled with sufficient margin can be explained by the limited authority of the electronic control system, as only a small part of the control surfaces are available. Thus, the issue lies on the aircraft design side which needs to come up with either larger control surfaces or more powerful actuators to achieve higher robustness. Nevertheless, for the conceptual study and an emergency landing system, these margins could be sufficient but need to undergo further and more detailed investigations.

Furthermore, the unstructured μ -synthesis yields interesting results that can be used in a further iteration of the control design. Even though it is hard to reduce the number of internal states of the unstructured controller to arrive at a simple linear control law for each virtual control, Table 2 indicates that there are cross coupling terms. In fact, these results indicate that v_{ϕ} should be a function of e_{ϕ} and e_r , v_{θ} should be a function of e_{ϕ} and e_{θ} , and v_r should be a function of e_{ϕ} and e_r . Those can be explained by both already proposed and implemented functions and physical relations. v_{θ} should include a turn compensation term, which compensated the reduced projected lift in a turn. Furthermore, v_r should include a turn coordination term as shown in (19).

Section 4.2 shows the nominal performance of the controller. It can be seen that the transient behavior is smooth and does not pose any unwanted bumps and maneuvers to the aircraft. Instead, the results indicate that enabling the electronic flight control system is a smooth process. Furthermore, after the emergency trajectory is planned, the aircraft is capable of tracking it. Additionally, redistribution of control surface deflections in case of an actuator failure works well and smooth and seems to be only limited by actuator limits and the fault detection performance. However, the results are limited by the assumption of an existing instantaneous fault detection module.

Although section 4.1 already looks at robust performance and stability, the analysis is done by means of linearized systems of the plant and the controller. However, this only allows an indication on the behavior of the nonlinear system but no definite statement. Thus, section 4.3 shows the response of the nonlinear system under the presence of model uncertainties. The values chosen are motivated physically instead of systemic. Again, the results indicate that the controller can handle the exposed uncertainties sufficiently well. However, the uncertainties chosen are smaller than usual for flight control design (see, e.g., [15]). Still, the results indicate that the controller has certain margins against model uncertainties. It is to be determined if these margins are sufficient for the final design of the aircraft and if a model accuracy within these uncertainty ranges can be achieved.

Section 4.4 investigates the disturbance rejection capabilities of the implemented flight control system and the proposed flight control laws. In the monte-carlo simulation, the aircraft is exposed to continuous wind turbulence with increasing wind speeds. The results suggest that starting from the lowest turbulences (at $20\,\mathrm{s}$), the turbulence noise is fed through to the actuation and flight state. However, the results indicate further, that the control laws are capable of limiting the effect of the disturbances. It can also be seen, that the aircraft behaves stable in all experiments and turbulence magnitudes. However, higher frequency control activity is required to do so.

6. Conclusion

This study shows the application of a hybrid NDI control law with optimization-based control allocation and failure handling to a semi-electrical split-flap configuration. The proposed control system is analyzed with respect to nominal and robust performance and stability with methods from robust control. Afterward, nonlinear time-domain simulations are used to show the performance of the system in nominal, failure, disturbance, or uncertainty conditions by using monte-carlo simulations. The system evaluation is used to draw conclusions about the applicability of a semi-electrical split-flap system to support general aviation emergency handling. The results indicate that the configuration under investigation is capable of handling the analyzed scenarios. However, the stability and performance margins are rather small due to the limited authority of the split control surfaces. However, since

this system will only be engaged in abnormal conditions, this may still be an acceptable trade-off. Nevertheless, further work is needed in order to address the open issues and questions.

7. Contact Author Email Address

daniel.milz@dlr.de

8. Acknowledgments

The funding of the *MOREALIS* project within the LUFO VI-1 framework (FKZ: 20Q1935E) by the German Federal Ministry for Economic Affairs and Climate Action (BMWK), is gratefully acknowledged.

Supported by:

Federal Ministry
for Economic Affairs
and Climate Action

on the basis of a decision by the German Bundestag

9. Copyright Statement

The authors confirm that they, and/or their company or organization, hold copyright on all of the original material included in this paper. The authors also confirm that they have obtained permission, from the copyright holder of any third party material included in this paper, to publish it as part of their paper. The authors confirm that they give permission, or have obtained permission from the copyright holder of this paper, for the publication and distribution of this paper as part of the ICAS proceedings or as individual off-prints from the proceedings.

References

- [1] Brian Pagán, Alex de Voogt, and Robert Doorn. Ultralight aviation accident factors and latent failures: A 66-case study. *Aviation, space, and environmental medicine*, 77:950–2, 09 2006.
- [2] R. Kuchar, W. Scholz, B. Dörfler, P. Herrmann, P. Jamakatel, J. Karger, J. Kiam, J. Klenner, M. Klennert, M. Lindlar, M. May, D. Milz, N. Mumm, D. Nospes, L. Peter, G. Looye, A. Schulte, and P. Stütz. Morealis a holistic approach to enhance safety for micro-aircraft operations. In *34th Congress of the International Council of the Aeronautical Sciences*, 2024.
- [3] Marc May, Daniel Milz, Werner Scholz, Peter Herrmann, Jonas Karger, Lars Peters, Nils Mumm, and Richard Kuchar. Mixed flight control layout for ultralight general aviation aircraft. In *34th Congress of the International Council of the Aeronautical Sciences*, 2024.
- [4] Jan Roskam and Samuel Henry. Synthesis of a separate surface wing leveler. *Journal of Aircraft*, 11(11):657–658, November 1974.
- [5] W. R. Bolton and D. J. Collins. General aviation application of separate surface stability augmentation. *Journal of Aircraft*, 12(10):826–829, October 1975.
- [6] Michael J. See and David Levy. The state of the art of general aviation autopilots. Technical report, NASA, 1980.
- [7] Yagiz Kumtepe, Tijmen Pollack, and Erik-Jan Van Kampen. Flight control law design using hybrid incremental nonlinear dynamic inversion. In AIAA SCITECH 2022 Forum, number 10. American Institute of Aeronautics and Astronautics, January 2022.
- [8] Daniel Milz, Gertjan Looye, and Marc May. Dynamic inversion: An incrementally evolving methodology for flight control design. *to be published*, 2024.
- [9] Daniel Milz, Marc May, and Gertjan Looye. Flight testing air data sensor failure handling with hybrid nonlinear dynamic inversion. In *EuroGNC 2024*, 2024.
- [10] T. S. C. Pollack and E. Van Kampen. Multi objective design and performance analysis of incremental control allocation based flight control laws. In AIAA SCITECH 2023 Forum. American Institute of Aeronautics and Astronautics, January 2023.

- [11] Daniel Milz, Marc Simon May, and Gertjan Looye. Dynamic inversion-based control concept for transformational tilt-wing evtols. In *AIAA SciTech 2024 Forum*, Januar 2024.
- [12] S. Sieberling, Q. P. Chu, and J. A. Mulder. Robust flight control using incremental nonlinear dynamic inversion and angular acceleration prediction. *Journal of Guidance, Control, and Dynamics*, 33(6):1732–1742, November 2010.
- [13] Xuerui Wang, Erik-Jan van Kampen, Qiping Chu, and Peng Lu. Stability analysis for incremental nonlinear dynamic inversion control. *Journal of Guidance, Control, and Dynamics*, 42(5):1116–1129, May 2019.
- [14] Daniel Milz and Gertjan Looye. Tilt-wing control design for a unified control concept. In *AIAA SCITECH 2022 Forum*. American Institute of Aeronautics and Astronautics, jan 2022.
- [15] Fabian Grondman, Gertjan Looye, Richard O. Kuchar, Q Ping Chu, and Erik-Jan Van Kampen. Design and flight testing of incremental nonlinear dynamic inversion-based control laws for a passenger aircraft. In 2018 AIAA Guidance, Navigation, and Control Conference. American Institute of Aeronautics and Astronautics, jan 2018.
- [16] Thomas Lombaerts and Gertjan Looye. Design and flight testing of nonlinear autoflight control laws. In *AIAA Guidance, Navigation, and Control Conference*, August 2012.
- [17] Eric N. Johnson and Anthony J. Calise. Pseudo-control hedging: A new method for adaptive control. In *Advances in NavigationGuidance and Control Technology Workshop*, 2000.
- [18] Sigurd Skogestad and Ian Postlethwaite. *Multivariable Feedback Control Analysis and Design*. John Wiley & Sons, 2001.
- [19] S. Bennani and G. Looye. Flight Control Law Design for a Civil Aircraft using Robust Dynamic Inversion. In *IEEE/SMC-CESA98*, pages 998–1004. IEEE, April 1998.
- [20] Federal Aviation Administration. Advisory circular ac 25.341-1: Gust loads, 2001. Accessed: 2024-07-01.